Applications in Energy and Combustion Science 20 (2024) 100300

Contents lists available at ScienceDirect

Applications in Energy and Combustion Science

journal homepage: www.elsevier.com/locate/jaecs

The impact of film cooling on the heat release within a rotating detonation combustor

Shreyas Ramanagar Sridhara [a,*], Antonio Andreini [a], Marc D. Polanka [b], Myles D. Bohon [c]

[a] University of Florence, Via Santa Marta 3, Florence, 50139, Italy
[b] Air Force Institute of Technology, Wright-Patterson Air Force Base, Dayton, OH, 45433, United States of America
[c] Chair of Pressure Gain Combustion, Technische Universität Berlin, Berlin, 10625, Germany

ARTICLE INFO

Keywords:
Detonation combustion
Film cooling
Rotating detonation combustor

ABSTRACT

Rotating detonation combustors establish a detonation wave that continuously circulates inside a small annulus. The presence of the detonation wave and the downstream oblique shock within the small annulus coupled with high mass flow induces a high heat load to the combustor wall. Preliminary analysis shows that for higher thermal power, internal air cooling alone is not sufficient to remove the heat out of the walls to maintain them below the maximum temperature of the metal. A possible solution is to use film cooling to reduce the heat flux to the combustor walls. One issue, though, is that the introduction of film cooling provides additional air into the system that can influence the combustion process as well as providing a location for secondary combustion.

This paper represents the first investigation to study the secondary implications on combustion of using film cooling in a rotating detonation combustor. The TU Berlin RDC architecture was modified with the introduction of 480 film cooling holes placed in the oblique shock region. High fidelity LES investigations were performed for different coolant plenum pressures to show the benefits of using film cooling. However, due to the presence of unburnt fuel in this post-detonation region, the coolant can result in additional combustion leading to an increase in temperature near the wall. One the one hand, these secondary reactions result in an increase of the overall heat release increasing combustion efficiency, however this also results in higher temperatures and reduced film cooling effectiveness. A simulation performed with nitrogen as a coolant enabled the effects of increased mixing caused by the ejection of coolant gases to be separated from the additional heat release. The simulation with nitrogen shows a reduction of 88% in the local heat release in the post detonation region resulting in similar performance as the uncooled case and significantly cooler walls.

1. Introduction

There are several configurations of Rotating Detonation Combustors (RDC), with different shapes [1] and sizes [2]. Among the most popular and widely used configuration is a cylindrical, annular RDC [3,4]. Fig. 1 represents the TU Berlin test rig which is designed to operate at a maximum thermal power of 2 MW. The flow field of an RDC, as shown in Fig. 1, is composed of a detonation front (the detonation region) with a trailing oblique shock (the oblique shock region) that continuously loops around this circular annulus. The oblique shock extends to the outlet and travels with the same speed in the laboratory frame of reference as the detonation, however the shock strength and relative Mach number is significantly lower. The fuel and air are supplied from the head end and the burnt gases are expanded out of the aft end. A sufficiently high mass flow rate of detonable mixture is required to sustain the detonation wave due to its high consumption speed. The bulk flow exiting the combustor is primarily axial with minimal tangential component [5].

RDCs are often made with a small annulus width, which aids in the sustaining and stabilizing the detonation wave [6]. The highly compressible and unsteady flow in the RDC, and high temperature gases close to the walls leads to peak heat transfer levels at least an order of magnitude greater than the conventional gas turbine (GT) combustors [7]. Numerous researchers have worked on characterizing the heat loads of an RDC. Braun et al. [7] developed a reduced order model to obtain the RDC flowfield and used a correlation to compute the heat flux. They obtained an average heat flux of 1 MW/m^2 for an RDC operating at one bar chamber pressure with the peak heat flux was observed at the triple point. Goto et al. [8] performed experimental analysis with an ethylene/gas-oxygen rotating detonation engine. They reported higher heat flux values up to 5 MW/m^2. Stevens et al. [9,10]

* Corresponding author.
E-mail address: shreyas.ramanagarsridhara@unifi.it (S. Ramanagar Sridhara).

https://doi.org/10.1016/j.jaecs.2024.100300
Received 30 June 2024; Received in revised form 1 September 2024; Accepted 12 October 2024
Available online 19 October 2024

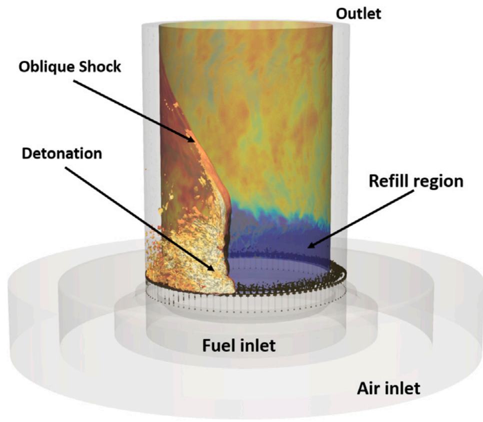

Fig. 1. Schematic of rotating detonation combustor.

performed measurements of bulk heat flux considering the instantaneous heat release and the mass flux as variables. The obtained results showed an average heat flux of 1.5 MW/m^2.

Recognizing the need to remove heat from an RDC to enable operation at steady state, Sandri et al. [11] performed a preliminary cooling requirement feasibility study and analysis. Their work revealed that an RDC cannot be cooled with only convective cooling by the combustion air. They suggested the need for film cooling with air to reduce the heat transfer to the wall and showed the nominal effectiveness that would have to be achieved. Overall, they suggested that film cooling can be a possible solution to reduce the heat thermal load on the RDC walls [11]. The issue would be understanding how the shock wave would interact with that cooling flow and how effective an air film thermal barrier could be.

A handful of researchers have begun studying film cooling numerically in an RDC. Tian et al. [12] performed CFD calculations of a premixed film cooled RDC. Both Tian et al. and Yu et al. [13] performed similar CFD analyses with one column of film cooling holes. Both investigations performed a complete three dimensional unsteady RANS combustion computation using Ansys Fluent. They looked at RDC trust performance and film effectiveness with varying the mass flow. While the time averaged temperature profiles show a benefit in using film cooling, due to the premixed injection configuration and simplified combustion model, these numerical investigations had no trace of unburnt fuel which could react with the coolant.

Other investigators like Rui et al. [14] performed numerical investigations on a rocket based detonation engine with film cooling. Their geometry consists of an RDC with a diverging nozzle and eight film cooling holes arranged as a single column. Similarly, their investigation was performed using ANSYS Fluent by solving unsteady reactive RANS equation with k-ω SST turbulence model. They specifically investigated different hole shapes with varying coolant velocity. They concluded that the elliptical holes enhance the interaction between the injected coolant flow and the axial mainstream flow, thereby obtaining a wider spread of the film.

Yu et al. [15] also studied the influence of film hole shape, specifically a cat ear shaped hole under various operating modes. Their RDC consists of two columns of film cooling holes with seven holes in each column. They also used ANSYS Fluent by solving reactive Navier–Stokes equations with the k-ϵ turbulence model. The outcome of their numerical investigation showed that the shaped holes provided superior cooling with reduced fluctuation in mass flow.

Shen et al. [16] studied the influence of film cooling hole inclination angle on the cooling performance of an RDC. They performed URANS simulations using their in-house solver utilizing a detailed chemical reaction model. Their simulated domain consisted of an RDC with premixed micro injection numerical model with four columns of film cooling holes surrounding both the outer and the inner wall. Their study shows that, increasing the hole inclination decreases the cooling performance along with coolant spreading. Furthermore, the addition of coolant decreases the height of the detonation wave.

There are a few experimental investigations of film cooling on a RDC. Chriss et al. [17] experimentally tested a six inch film cooled RDC. Their investigations revealed that, the coolant mass flow influenced the engine operability. As the coolant mass flow increased, the combustor experienced more unstable modes. The rate of temperature increase and the acoustic modes were governed by the coolant mass flow. Yu et al. [18] performed experimental investigations of shaped film cooling holes on a hollow RDC. They noticed that the film cooling has no influence on the propagation velocity of the detonation wave. Moreover, the obtained temperature patterns were similar to their computational simulations.

The successful integration of RDC to a gas turbine demands an efficient means to cool the walls. Thermal management and optimization of cooling systems for GT engines is important because it has an impact on overall efficiency. All the available investigations in the literature were performed in a premixed configuration. Furthermore, their investigations include just one or two columns of film cooling holes, and the investigations were performed by solving unsteady RANS equations. A detailed investigation with an RDC cooled around the full annulus with film cooling is currently lacking in the literature to understand the full implications of the shock interaction with the coolant flow. Furthermore, simulations that are not premixed are needed to quantify the effects of residual fuel interactions with the oxygen rich cooling flow. Predicting mixing in any combustion simulation is the key for obtaining accurate information. URANS simulations with any of the turbulence models fail to capture the significant vorticity structures that affect the mixing. Moreover, the turbulence chemistry interactions are computed using the turbulence models which assume isotropicity.

Large Eddy Simulations (LES) on the other hand resolve most of the turbulent scales which provides more information about the mixing and accurate turbulence chemistry interaction [19]. In the RDC, the detonation performance is more sensitive to the reactive mixture quality. Therefore, high fidelity simulations are needed to predict the mixing in the refill region and the mixing of the coolant gases. In this context, LES are performed on the TU Berlin RDC with film cooling holes around the full annulus of the combustor. The average gas temperature profiles near the wall along with the variation in coolant mass flow and the hot gas ingestion response are discussed in detail.

2. Film cooling configuration

The non premixed TU Berlin RDC architecture shown in Fig. 1 was implemented with film cooling to perform high fidelity simulations. An earlier investigation of the TU Berlin RDC in an uncooled configuration was performed by Nassini et al. [20] that verified the computations were matching the experimental results. The simulated domain includes both the fuel and air plenum connected to the injectors. For this RDC, there were radial air gap injector with a width of 1 mm and 100 axial fuel injector holes with a diameter of 0.5 mm placed in a jet in cross flow configuration. For this investigation, the feed pressure for the air was 7.0 bar creating a mass flow of 430 g/s. The fuel plenum delivered hydrogen at a pressure of 13.5 bar resulting in an equivalence ratio of one for the combustor.

The height of the refill region was measured to be around 4 cm. The region below 4 cm is termed as the detonation region because of the presence of the high pressure detonation wave. The region above 4 cm is the oblique shock region. For the current investigation, the film cooling holes were distributed only in the oblique shock region within the region highlighted by the white dotted lines in Fig. 2. The detonation region was excluded to reduce the possibility of detonation quenching due to reactant dilution caused by coolant mixing. Furthermore, Tien

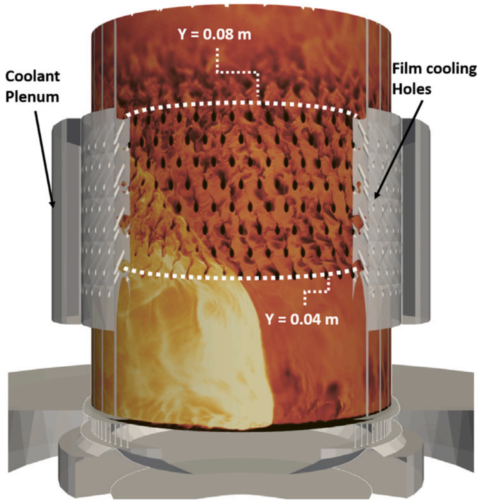

Fig. 2. Film cooled TU Berlin RDC.

et al. [12] observed hot gas ingestion into the coolant plenum in the detonation region, so this region was avoided.

The highlighted region in Fig. 2, extending from 4 cm to 8 cm, was populated by the film cooling holes with a diameter (Φ) of 1 mm and an inclination of 30°. A classical staggered arrangement with a pitch of 5.8Φ in X and 4.7Φ in the Y direction was applied. With this distribution scheme, the combustor was covered with a total of 480 holes. These holes were fed from a coolant plenum where the coolant entered the domain from the bottom of the plenum. The coolant plenum pressure (P_{cool}) was chosen based on the circumferential distribution of static pressure at the axial position of 4 cm where the first row of film cooling holes are situated. Due to the oblique shock, the peak pressure reaches a maximum of 5.5 bar and the lowest pressure is in front of the oblique shock which corresponds to 1.4 bar. The average pressure over the cycle was calculated to be 2.4 bar. To ensure a positive coolant supply, the plenum pressure should be greater than the average pressure. To assess the influence of coolant mass flow on the RDC flow field, and to investigate its impact on the detonation wave, three different coolant mass flows were chosen. This was achieved by imposing pressures of 2.75, 3.0, and 3.5 bar in the coolant plenum. The achieved coolant mass flow corresponds to 9, 16, and 26% of the combustor core flow.

3. Numerical model

Large Eddy Simulations were performed using the AVBP code developed by CERFACS. The solver has been extensively validated for various unsteady cases including film cooling [21–24]. AVBP solves fully compressible, multispecies, reactive Navier–Stokes equations. It uses different solving schemes like Taylor-Galerkin TTG4 A (Fourth order in time and third order in space) and Lax Wendroff (second order in space and time). The explicit time integration is carried out enforcing a dynamically maximum CFL of 0.7 resulting in a timestep of 6×10^{-9} s. The WALE LES model along with the localized artificial diffusivity model is used to stabilize the solving scheme. The hydrogen air detonation is modelled using 4S1R single step reaction scheme developed by Nassini et al. [20]. The current reaction mechanism is compatible with the Lax Wendroff convection scheme. The single step reaction mechanism uses four species H_2, O_2, H_2O and N_2 in a single reaction.

The computational domain included the TU Berlin RDC test rig along with the injectors, plenums, and film cooling holes. The combustor was designed with an annulus width of 7.6 mm and an outer wall diameter is 90 mm. The combustor operated with hydrogen and air. The TU Berlin RDC test rig included 100 fuel injectors with a diameter of 0.5 mm and a circumferentially constant airgap of 1 mm for air supply inside the combustion chamber. The test rig was fully discretized with a pure tetrahedral mesh with an overall mesh count of 380 million elements. The fuel injectors were discretized with a spacing of 80 μm along with 170 μm for the air gap and the refill region which covers 20 mm starting from the injectors. The coolant holes were discretized with a spacing of 300 μm and their surrounding regions with 450 μm as shown in Fig. 3.

The calculations were performed on a HPC cluster at the University of Florence. The cluster nodes count two 32 core AMD processors clocking 2.5 GHz. Due to the mesh size and a small time step, each simulation required 200,000 CPU hours. The choice of the grid sizing, timestep, wall models and boundary conditions were based on the previously performed validation by Nassini et al. [20]. Non-reflecting Navier–Stokes characteristic (NSCBC) was used for inlets specifying pressure and temperature to obtain the desired mass flow. The outlet pressure of 101325 Pa was set with the NSCBC pressure outlet boundary condition [25].

The current study was an initial evaluation of film cooling in RDC. This study focuses on the fluid dynamics and specifically the reactivity of the fuel with the film and not the heat transfer to the walls. Hence, the walls were modelled with turbulent adiabatic wall functions available on AVBP which gives an advantage of not using prism layers to capture the boundary layer. The wall models implemented in AVBP were validated for different flow fields including film cooling applications [21,26]. Several researchers have used the same approach for film cooling cases. Namely, Aillaud et al. [27], Shum-Kivan et al. [28], and Agarwal et al. [29] have each performed film cooling simulations by specifying adiabatic no slip walls.

To initiate the detonation, the hot combustor flow field was interpolated from the previous simulation without film cooling [20]. The obtained Celik's quality index for the current grid is shown in the right image of Fig. 3. The Celik's quality index [30] is calculated using Eq. (1) where QI_v is the quality index, μ_{sg} is the sub grid viscosity, and μ is the molecular viscosity. The quality index in the refill region was found to vary between 0.7–0.9, while in the film cooling region it was found to be between 0.9–1. Both the quality index and the y^+ values for the simulations performed were within the acceptable ranges, which is indicative of an appropriate large eddy simulation. The y^+ values were verified to be in the proper range (30–300) from previous wall model simulations. The average y^+ in the film cooling region varied between 30 to 40 while in the detonation region they were in the range of 20 to 80. The maximum and minimum y^+ in the detonation region correspond to 2 and 150 near the detonation, respectively.

$$QI_v = \frac{1}{1 + 0.05\left(\frac{\mu_{sg}}{\mu}\right)^{0.53}} \tag{1}$$

4. Heat release results

With a chamber mass flux of 290 kg/sm^2, the TU Berlin RDC always operates in a single wave mode [4]. A large eddy simulation investigation at this operating point reveals that the detonation wave has a height of approximately 4.5 cm. The detonation wave and the oblique shock is observed and depicted as a phase averaged temperature contour in Fig. 4(a). The detonation wave is positioned at π. The low temperature region, represented by the blue colour, is the refill region where the fresh gases injected from the injectors are mixed before being consumed by the detonation wave.

To analyse the mixing in the refill region, a contour of phase averaged hydrogen mass fraction is shown Fig. 4(b). The current numerical test point operates at an overall equivalence ratio of 1.0, which corresponds to a hydrogen mass fraction of 0.029. As previously observed, the distribution of the hydrogen mass fraction in the refill

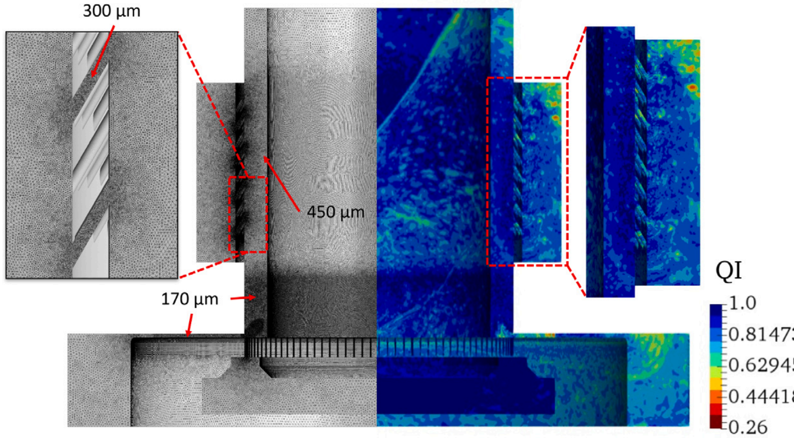

Fig. 3. Section of mesh grid used for simulation and the obtained Quality Index after the combustion simulation.

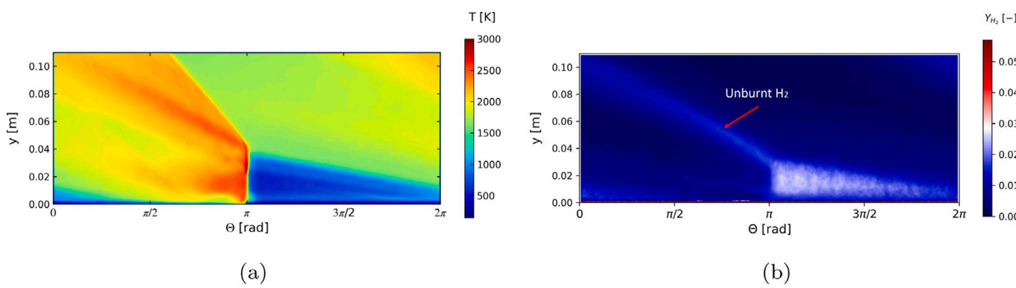

Fig. 4. Phase average (a) Temperature contour and (b) Hydrogen mass fraction for uncooled (No Film) RDC.

Table 1
Summary of the case runs and the obtained flow quantities.

P_{cool} [bar]	$\dot{m}_{air}$ g/s	$\dot{m}_{fuel}$ g/s	$\dot{m}_{coolant}$ g/s	*Mass ratio* %	$P_{chamber}$ [bar]	*Detonation height* cm	$\frac{P_{cool}}{P_{chamber}}$ –
No Film	430	13.2	0	0	1.3	4.5	0
2.75	430	13.2	40	9.3	1.55	4	1.77
3	430	13.2	68	15.8	1.7	3.5	1.76
3.5	430	13.2	112	26	2	3	1.75

region shows a wide variation in the equivalence ratio due to the unmixedness caused by the injector configuration as detailed by Nassini et al. [20]. Additionally, a hydrogen rich buffer region occurs due to a faster responding fuel injector, compared with the air injector. Due to the unmixedness, the combustion process does not consume all the injected hydrogen resulting in unburnt hydrogen leaking past the detonation along the slip line as shown in Fig. 4(b).

4.1. Implications of oxidizer mass addition

The current film cooled RDC shown in Fig. 3 adds additional oxidizer into the combustor. When the coolant comes in contact with the hot gases, secondary burning occurs providing additional heat release. To further analyse the affect of this heat release on the performance of a film cooled RDC, three different coolant mass flow rates were implemented. These were achieved by imposing three different coolant plenum pressures, P_{cool}, as reported in Table 1. For a plenum pressure of 2.75 bar, the achieved coolant mass flow was 40 g/s. Similarly, for P_{cool} of 3.0 bar and 3.5 bar, this corresponds to 68 and 112 g/s, respectively. The ratio of coolant mass flow to the combustor mass flow is reported as mass ratio in Table 1. Due to the small combustor volume and high Mach number in the chamber, any addition of mass flow will increase the chamber pressure from the uncooled value of 1.3 bar, serving to further pressurize the combustor. For 40 g/s of coolant, the obtained mass ratio was 9.3% which imposes a chamber pressure of 1.55 bar. For mass ratio of 15.8% and 26%, the obtained chamber pressure was 1.7 and 2.0 bar, respectively.

The increase in chamber pressure has an impact on the detonation. As the chamber pressure increases, the height of the detonation decreases. This is consistent with other investigations where the back pressure was increased with the addition of an aerodynamic nozzle or restriction at the exit. Studies like Ramanagar et al. showed that as the back pressure increased due to an area restriction, the detonation height decreased. [31].

For the uncooled combustor, the detonation wave was observed to be a straight standing wave with a height of approximately 4.5 cm. With film cooling, for a coolant mass of 40 g/s, the increase in chamber pressure modifies the shape of the detonation. A backward leaning detonation wave was observed with a height of 4.0 cm. As further coolant is added to the combustor, the backward leaning shape becomes more prominent along with the decrease in detonation height. For a coolant mass flow of 68 g/s, the detonation height was observed to be 3.5 cm, while for 112 g/s the obtained height was approximately 3.0 cm.

The gas temperature contours obtained adjacent to the adiabatic outer wall containing the film cooling holes are shown in Fig. 5. The detonation wave is moving from left to right and is positioned at π for all the contours. For film cooling cases, the film cooling holes start at an axial position of 4 cm and cover the region until an axial position of 8 cm. The change of the detonation shape along with the oblique shock wave interacting with the coolant flow is clearly visible. In these

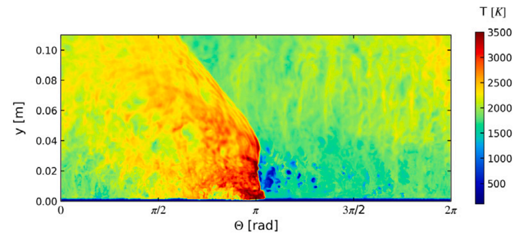

(a) No Film

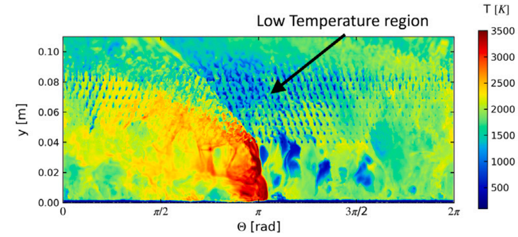

(b) $\dot{m}_{coolant} = 40$ g/s

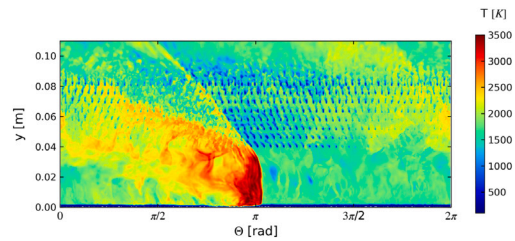

(c) $\dot{m}_{coolant} = 68$ g/s

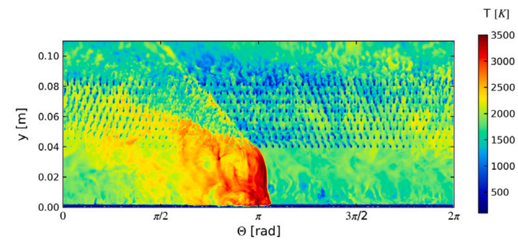

(d) $\dot{m}_{coolant} = 112$ g/s

Fig. 5. Temperature of the outer wall revealing the impact of the detonation on the film cooling for the three cooling pressure levels.

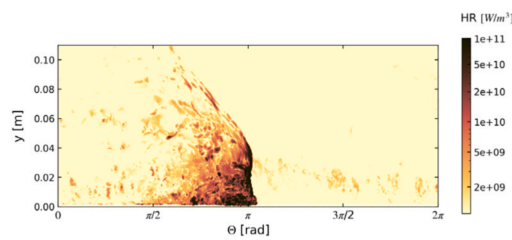

(a) No Film

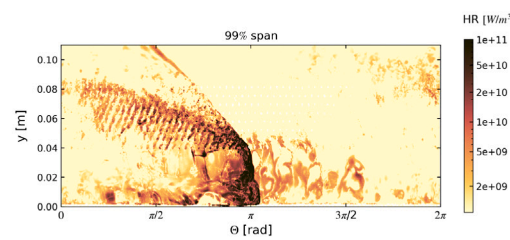

(b) $\dot{m}_{coolant} = 40$ g/s

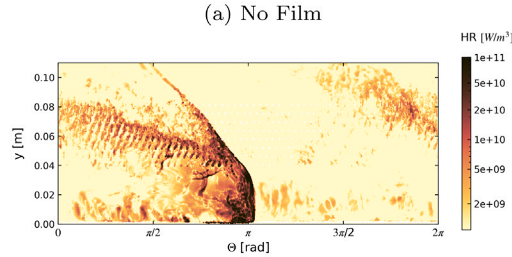

(c) $\dot{m}_{coolant} = 68$ g/s

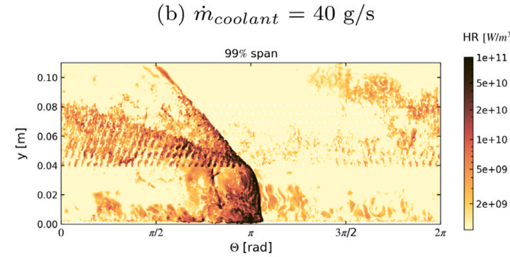

(d) $\dot{m}_{coolant} = 112$ g/s

Fig. 6. Contour of heat release obtained on the outer wall for all the cases.

contours, the lowest temperature is always observed to be just ahead of the oblique shock as labelled in Fig. 5(b). This is because of the circumferential variation of the chamber pressure due to the presence of the oblique shock wave. This causes the coolant supply mass flow to not be uniform throughout the cycle. The oblique shock disrupts the film and blocks the coolant supply for part of the cycle. However, due to the higher plenum pressure, the coolant supply recovers, reestablishing the coolant film downstream of the oblique shock.

Moreover, the presence of oxygen in the coolant reacts with the hot unburnt hydrogen providing heat release close to the outer wall. This deflagrative burning due to the additional reactant injection increases the temperature near the wall. Hence, the local temperature contours in the region of the film cooling holes is not always lower in temperature for all portions of the cycle. However, as the coolant supply increases, more mass flow is available for protecting the walls. This resulted in lower temperatures in the coolant hole region as the coolant mass flow increases.

The contour of heat release obtained on the outer wall is shown in Fig. 6. As in the temperature contours of Fig. 5, the detonation is located at the position π. The peak heat release was always found to be in the detonation wave region and is always in the order of magnitude of 3.4–4.4 × 10^{12} W/m^3. In contrast, the deflagration heat release found further downstream is in the order of magnitude of 3–10 × 10^9 W/m^3. Therefore, the heat release contours shown are scaled to the values found for deflagration to highlight the impact of the secondary combustion. For the uncooled case, the deflagration is observed to primarily occur along and just downstream of the oblique shock. The oblique shock results in a thin line of deflagrative heat release due to the increase in pressure and temperature behind the shock, which enhances the reactivity of the mixture. This is evident for all four cases.

For the film cooled RDC however, a greater amount of secondary heat release was observed due to the reaction of coolant with the hot unburnt hydrogen. For a lower coolant mass flow, i.e. 40 g/s, greater deflagration heat release was observed closer to the detonation wave above 4 cm followed by heat release due to coolant burning. An increase in parasitic combustion was also observed in the refill region. As the mass flow was increased to 68 g/s, the region of coolant burning increased and heat release due to deflagration above an axial position of 4 cm is greater. The highest deflagration heat release was observed with the coolant mass of 112 g/s due to the high availability of oxygen for secondary reaction. For this case, one can see the clear patterning of the heat release mirroring the array of cooling holes.

Interestingly, this region of high heat release occurs behind the oblique shock. This is attributed to the fact that the cooling flow is effectively closed off with passing of the oblique shock as was shown in more detail in Ramanagar Sridhara et al. [31]. The oblique shock elevates the local pressure above the plenum pressure thus not allowing coolant to enter the detonation channel. The secondary reactions do not occur until the coolant flow is reestablished. As the coolant is reintroduced from the holes, it mixes with the hydrogen present in the free stream flow and burns locally. This is similar to the secondary burning phenomena seen by Polanka et al. [32,33] in a non-detonating environment. Due to the disruption of the film by the oblique shock, the coolant deflagration in the region trailing the shock from approximately 0 to $\pi/2$ happens closer to the wall. As the coolant flow reestablishes, a full layer of coolant protects the near wall region and lower heat release on the outer wall occurs as seen in the region from π to 2π. The deflagration burning happens further away from the wall due to the higher penetration of coolant into the hot gas stream as was documented by Ramanagar Sridhara et al. [31].

4.2. Heat release along the span

The coolant penetration into the combustor and the position of coolant burning can be visualized using the circumferentially averaged heat release profiles obtained across different radial spans. The detonation and the oblique shock pass over the holes with a frequency of 7.5 KHz, which corresponds to a wavespeed of 98% CJ velocity. This caused the film layer to be disrupted and rebuilt at this same frequency. This phenomenon was discussed in more detail in Ramanagar Sridhara et al. [31] including the fact that unburned fuel can propagate into the film cooling holes for part of the cycle. The quantities are averaged across 30 detonation cycles with a sampling time of 10 μs.

To obtain the circumferentially averaged heat release profiles, several cut planes were created at different radial spans as shown in the top image of Fig. 7. The 97% span corresponds to a radial position closer to the outer wall where the film cooling holes are placed. Three other positions moving closer to the inner wall at 75% span, 50% span and then at 25% span were also interrogated to understand how the film cooling penetrated across the width of the detonation channel. The upper image represents the average heat release across the channel width for a plenum pressure of 3.5 bar. The shaded regions in the subsequent plots in Fig. 7 corresponds to the axial positions of film cooling holes, namely between 4 cm and 8 cm.

The magnitude of heat release due to detonation is similar for all the given cases at 97% of the span. However, the height of the detonation, as estimated by identifying the axial location at which the heat release profiles decrease below 10^3 MW/m^3, decreased as the amount of cooling increased. At midspan, for an uncooled RDC, this axial location was observed to be 4.5 cm. For the cooled cases, as the pressure in the coolant supply was increased to 2.75, 3.0, and 3.5 bar, the detonation wave height was reduced to 4.0, 3.5, and 3.0 cm, respectively. This is attributed to the higher chamber pressure as discussed previously.

Downstream of the detonation wave in the uncooled combustor, the heat release decreases along the axial length. However, due to the reaction of oxygen in the coolant with the unburnt hydrogen, an increase in heat release for all the film cooled cases was observed. This increase began at an axial position of 4.0 cm where the first row of film cooling holes were situated. Heat release in the film region is greater as the coolant pressure was increased due to the higher mass flow of coolant. This heat release has an impact on the wall temperature and overall performance of the RDC. The axial locations of the film cooled holes are also apparent as peaks and valleys in the heat release profiles.

For the 75% span location, the circumferentially averaged heat release in the detonation region follows the same trend as at 97% span. However, the magnitude of heat release is higher than at the 97%. The detonation heat release increases at a lower radius because of the fuel mixture stratification at lower radius created by the current injection scheme [20]. In the film cooling region, the heat release of the uncooled RDC is still less than the film cooled RDC. However, the magnitude of the deflagrative heat release due to the film cooling is about 66% less than observed at 97% span. This shows that the coolant does reach 75% span, causing additional burning at this span, but not at the magnitude found near the wall. Higher heat release was observed for 3.5 bar due to the higher mass flow inducing greater penetration into hot gas stream with respect to the other cases. The coolant plenum pressures of 3.0 and 2.75 bar have similar trends and magnitudes.

Moving towards a lower radius (i.e at mid span) the overall magnitude of heat release increases further in the detonation region. At this span, the heat release of the cooled cases are higher at certain axial locations in the detonation region. This is attributed to the shorter, stronger detonation wave due to the increased chamber pressure. In the film region, the heat release of the film cooled RDC is still greater than the uncooled RDC due to the deflagration burning. Although the heat release for the film cooled cases are another 50% lower then at 75% span and are now close to the uncooled level. The heat release for the 3.5 bar case remains the highest when compared to the other cases suggesting the coolant might penetrate up to 50% span or at least the effects of additional oxygen being mixed into this region are felt.

At the 25% span, near the inner wall, the circumferentially average profiles are closer together and just slightly higher than the uncooled RDC. Again this is attributed to the increased chamber pressure forming a stronger detonation. The decrease in heat release follows the same trend for all the cases; however, at different axial locations. This is again due to the influence of chamber pressure on the height and shape of the detonation. Although, the heat release profile decreases throughout the axial length, the film cooled cases still exhibit a higher heat release than the uncooled combustor.

5. The impact of coolant burning

The deflagration reaction between the coolant and the unburnt hydrogen creates an unique situation inside the RDC. Specifically the question arises as to whether the reaction is promoted by the physical presence of additional oxygen or if it is facilitated by the additional mixing that the film cooling jet creates. To assess the influence of coolant burning, and to better understand the role of coolant penetration on the mixing enhanced reactivity, a simulation was performed with nitrogen as the coolant. The 3.0 bar plenum pressure was chosen to create a reasonable mass flow without the ingestion problem of the 2.75 bar case.

The resultant heat release contours on the outer wall for 3.0 bar with air and nitrogen are shown in Figs. 8(a) and 8(b), respectively. The contour range is set to highlight the deflagration heat release. The heat release with nitrogen coolant shows a significant reduction throughout the film cooled region, i.e. above the axial length of 4 cm. There is still some secondary heat release, namely along the oblique shock path, that can be attributed to enhanced reaction rates due to the local increase in temperature and pressure after the shock. However, it is apparent that the significant secondary burning that occurred near the film cooling holes when air was ejected is no longer present for the nitrogen case.

This phenomena of secondary burning near film cooling holes in a fuel rich environment was discussed by Polanka et al. [32,33] in a gas turbine environment. They showed that the oxygen present in a film cooling hole can stabilize a flame locally downstream of the injection site. The current investigation reflects a similar reacting situation and similar to their results, cooling with nitrogen removes the secondary burning. Furthermore, there is a reduction in the amount of secondary burning with downstream distance. This is similar to the results of Shewhart et al. where the build up of coolant from the first couple

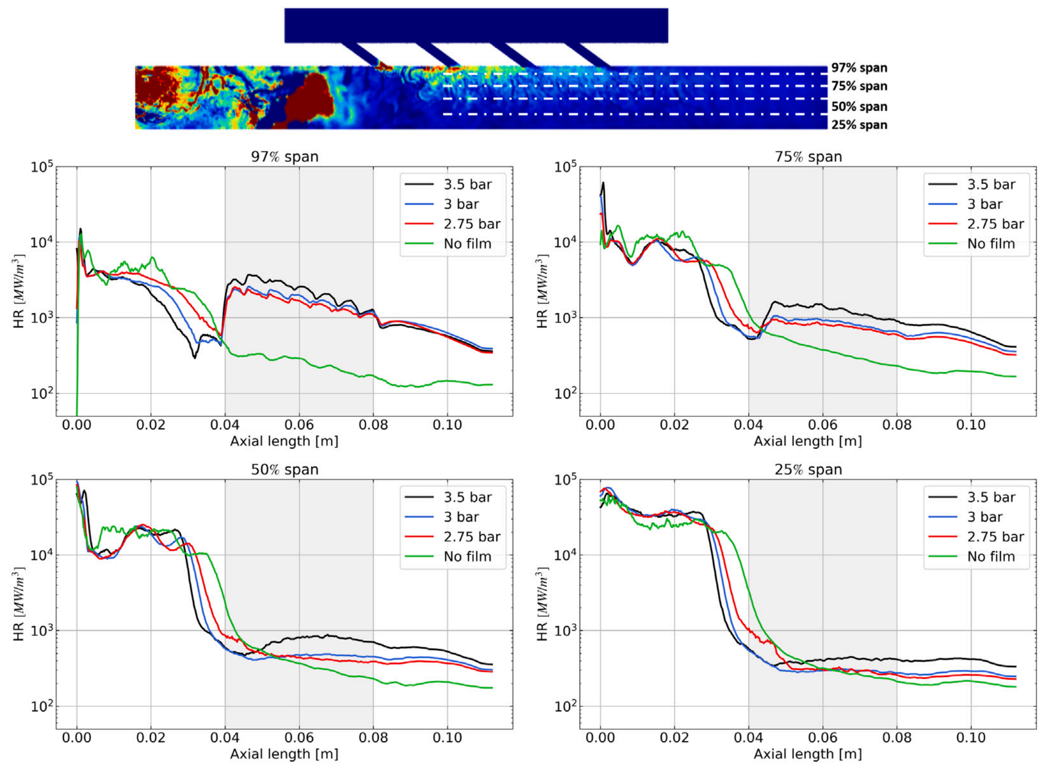

Fig. 7. Temporal and circumferentially averaged heat release profiles across 25, 50, 75 and 97% of radial span for all the cases.

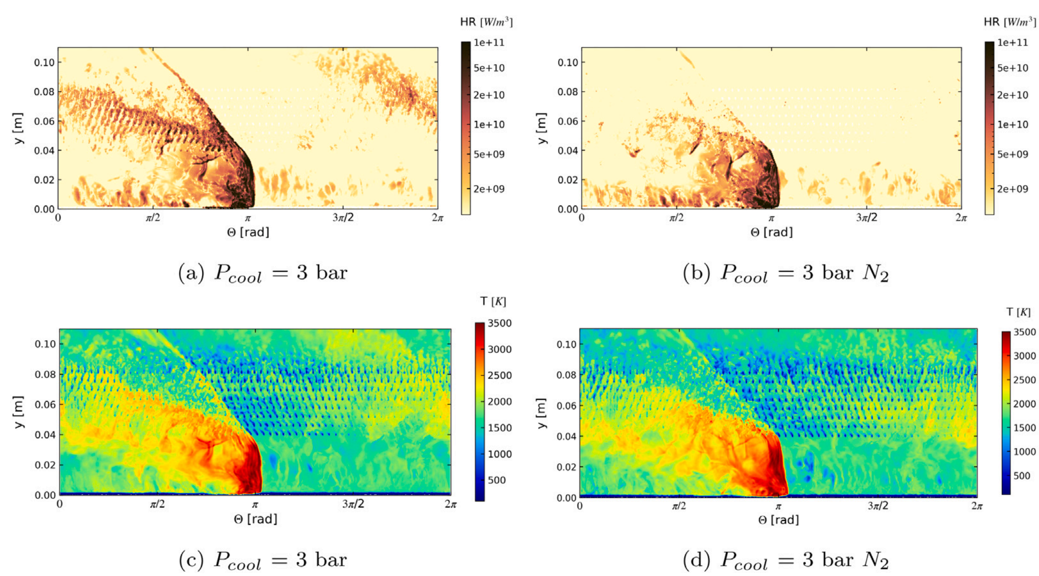

(a) $P_{cool} = 3$ bar

(b) $P_{cool} = 3$ bar N_2

(c) $P_{cool} = 3$ bar

(d) $P_{cool} = 3$ bar N_2

Fig. 8. Heat release contour obtained on the outer wall for a plenum pressure of (a) 3 bar and (b) 3 bar with N2. Temperature contour of (c) 3 bar and (d) 3 bar N_2 case obtained on the outer wall.

of rows both protects the downstream wall from further reaction and pushes the heat release off the wall downstream [34].

Temperature contours obtained on the outer wall are shown in Figs. 8(c) and 8(d). As expected, the shape of the detonation remains the same for both the coolant cases. The post detonation gases follows the same path for nitrogen and air. This shows that the film development after being disrupted by the oblique shock remains largely unchanged. However, a greater reduction in wall temperature is observed for the nitrogen case. This is because the nitrogen is allowed to cool the wall without bringing additional heat release to the outer wall [32].

The circumferentially averaged hydrogen mass fractions is plotted in Fig. 9. Three cases are considered including: the no film (uncooled case), the 3.0 bar with air as coolant, and 3.0 bar with nitrogen as coolant. The unburnt hydrogen mass flow $\dot{m}$ at an axial position of 4 and 8 cm is reported in Table 2.

Regardless of the coolant composition, the hydrogen mass fraction at 4 cm is 7% lower for the film cooled case than the case without film. This suggests that the increased coolant plenum pressure resulted in an increase in hydrogen consumption in the detonation region. While not shown here, the presence of the film cooling probably also had an effect on the mixing characteristics in the detonation region. As Nassini et al. [20] previously showed, the mixture ahead of the detonation

Table 2
Unburnt hydrogen mass flow at an axial position of 4 cm and 8 cm.

P_{cool} [bar]	$\dot{m}_{f_4}$ [g/s]	$\dot{m}_{f_8}$ [g/s]	H_2 Reduction [%]
No Film	2.30	1.57	31.7
3	2.10	1.19	43.1
3 N_2	2.05	1.38	33.2

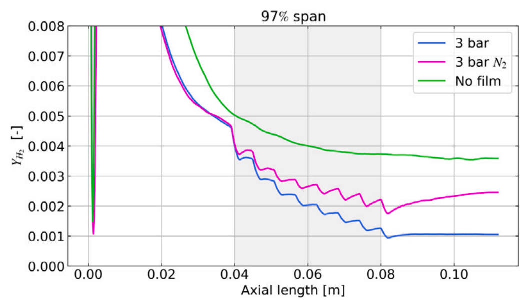

Fig. 9. Circumferentially averaged hydrogen mass fraction profiles for 97% span.

was quite inhomogenous, and consequently the detonation products contain portions with significant amounts of unburned hydrogen and other portions with significant residual oxygen as seen in Fig. 4(b).

From Table 2 and in Fig. 9, the mass fraction of hydrogen continually decreases through the film cooled region. This can be attributable to two effects. First, the film cooling jets can enhance the mixing between products originating ahead of the film cooling region. The fact that both the nitrogen and air coolant result in the same level of mixedness is expected. This can account for the 33% reduction in the hydrogen mass fraction. However, the additional 10% drop seen in Table 2 is due to the second reason. Namely, the mass addition of oxidizer providing an increased reaction rate for the residual hydrogen. This is seen in the lower level of hydrogen mass fraction in the film cooled region for the air injection as compared to the nitrogen.

5.1. Impact of mass addition of air on heat release

To quantify the contributions to the heat release and the resultant gas temperature, the circumferentially averaged heat release profiles are plotted in Fig. 10. At 97% span, the heat release of 3.0 bar with air and nitrogen are similar in the detonation region. This is reflected in that the chamber pressure is the same (1.7 bar) for both cases providing the same height and shape of the detonation wave. In the film cooled region, the heat release due to deflagration is reduced by 80% for the nitrogen coolant, confirming that the additional oxygen has a substantial effect. However, the heat release for the nitrogen cooling case at 97% span is still 50% greater than the uncooled case up to an axial position of 7 cm. This is attributed to the increased reaction rate due to the increased turbulence provided by the injection process. After the axial length of 7 cm, the heat release of the nitrogen case is less than the uncooled RDC due to the effect of reduced reaction caused by dilution of reactive mixture with nitrogen coupled with the additional consumption of unburnt hydrogen prior to this location.

It is worth noting that even with additional heat release in the film cooling layer, the resultant gas temperature profiles reflect that the air cooling film is able to protect the outer wall. At 97% span, for the uncooled case, the gas temperature has only dropped from 2200 K to 2100 K at the axial position of 8 cm. Whereas the air cooled combustor has reduced the temperature along the outer wall down to 1400 K. Moreover, the nitrogen cooled RDC obtains an even greater reduction in temperature of 1300 K at 8 cm. This delta in temperature from the air to the nitrogen cooled cases can be attributed to the reduced heat release in the layer. At the combustor outlet (i.e. at the axial location of 11 cm) both film cooled cases show an increase in gas temperature due to the lack of additional cooling holes and the diffusion of the film. But both cases are still 500 K lower than the uncooled case. This shows that while nitrogen (or a coolant without oxygen) would be preferred in an RDE, the additional heat release caused by the addition of oxygen is manageable.

The heat release at 75% span follows the same trend as at 97% span. In the film cooled region, the overall level of heat release for the air cooled case is about half the level it was at 97%. Also, the nitrogen cooling case exhibits the lowest heat release; even lower than the uncooled combustor. This reveals the additional benefit of nitrogen dilution on the process. Looking at the gas temperature at 75% span, a similar profile is experienced until an axial position of 5 cm. At this location, the film starts to have an influence giving some insight into both the penetration of the coolant jet and the build up of the coolant from the earlier rows. After this location, the nitrogen coolant again shows a greater reduction in temperature. However, the change was only from a temperature of 1900 K for the uncooled case to 1800 K for the air cooled configuration and 1700 K with nitrogen. This shows that the film has an affect on the gas temperature of more than 25% of the span, but its impact is reduced away from the wall.

5.2. Overall heat release due to film cooling

To characterize the heat release in terms of detonation and coolant deflagration, the RDC is divided into three regions as shown by the left image of Fig. 11. Region 1 extends up to the beginning of the film holes (4 cm). Region 2 covers the film cooling holes, starting from 4 cm and extending to 8 cm. Region 3 starts at 8 cm and ends at the outlet. The volume averaged heat release for the different regions are plotted in log scale shown on the right image of Fig. 11. The magnitude of heat release due to detonation is high since it is the primary mode of combustion.

For the uncooled RDC in Region 1 the heat release is of the order of magnitude of 1.7×10^{10} W/m^3. Region 2 and 3 experience only deflagrative combustion at a reduced heat release of 5.3×10^8 and 2.7×10^8, respectively. On the other hand the film cooled RDC experienced more overall heat release. For a plenum pressure of 2.75 bar, the heat release in Region 1 was observed to be similar to the uncooled RDC. Whereas in Region 2 and 3, due to the coolant burning, the heat release increased to 8.6×10^8 and 4.8×10^8 W/m^3, respectively. For a plenum pressure of 3.0 bar, the reduced detonation height increased the heat release in Region 1 even more above the 2.75 case. Region 2 and 3, due to the introduction of more oxygen than at 2.75 bar, again increased the heat release an additional 2% higher. The highest heat release in all the regions was observed for the 3.5 bar plenum pressure case. At a coolant mass flow of 112 g/s and the increased chamber pressure of 2 bar, the heat release in Region 1 was 2.0×10^{10} W/m^3.

Running the RDC with nitrogen coolant yielded a similar heat release in Region 1 as the 3.0 bar with air coolant. As expected, the nitrogen coolant had a reduced heat release in Region 2 and 3 with respect to the air coolant. Comparing the nitrogen cooled case against the case without film cooling, the overall heat release across the full span in Region 2 was nearly the same. However, due to the reduction in hydrogen concentration in Region 1, the overall heat release was still higher for the film cooled case.

6. Overall performance of the film cooled RDC

A key issue was understanding how the film cooling interacted with the unburned hydrogen. To investigate this, the percentage of the inlet hydrogen mass fraction that remained at the outlet was determined and is reported in Table 3. For the uncooled combustor 12.3% of the amount of hydrogen injected at the RDC inlet is not combusted and remains at the combustor outlet. For the film cooled RDC, as the plenum pressure is increased, a greater amount of hydrogen is consumed. Clearly the

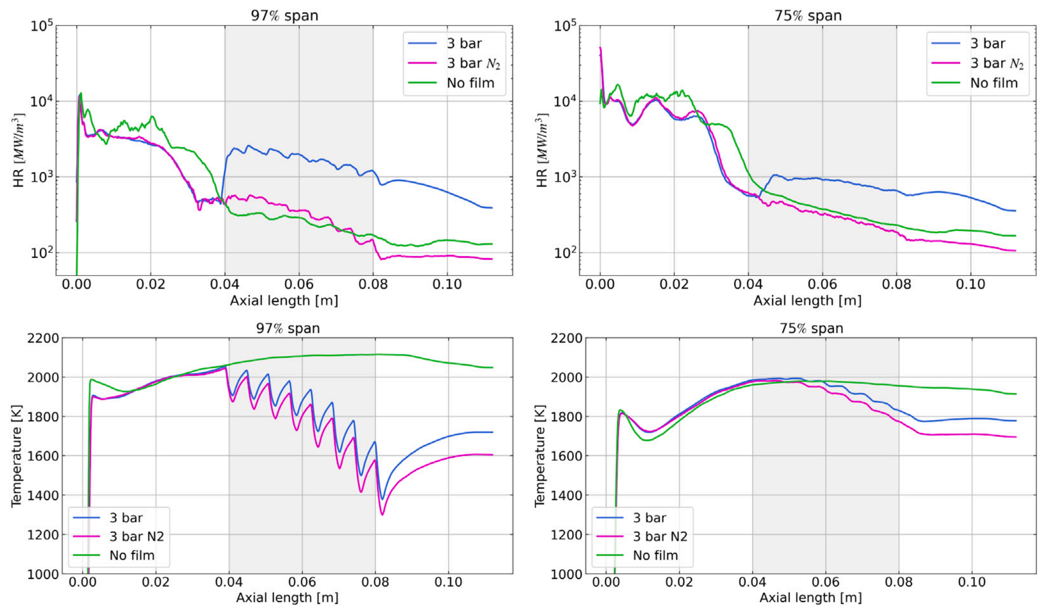

Fig. 10. Circumferentially averaged heat release profiles on the top and temperature profiles on the bottom for 97% and 75% span.

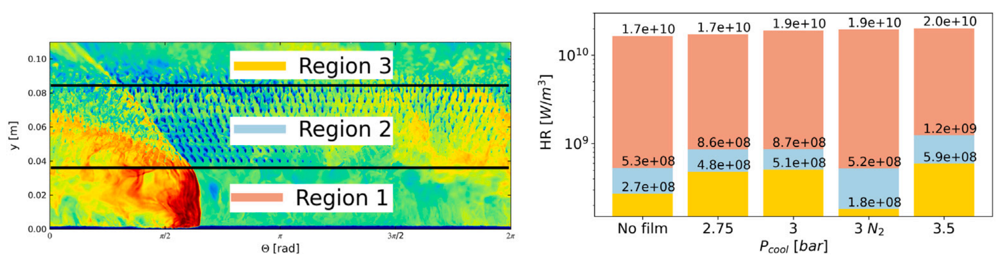

Fig. 11. Temperature contour on the left, representing the division of RDC into three regions and characterization of heat release with respect to the three regions on the right.

Table 3
The amount of unburnt H_2 at the exit, the outlet temperature, and the combustion efficiency for all the cases.

Pcool [bar]	Unburnt H_2 [%]	Outlet temperature [K]	η_c [%]
0	12.3	1900	90.5
2.75	8.0	1874	93.2
3	7.6	1832	94.4
3 N_2	11.4	1761	90.7
3.5	6.6	1771	96.8

addition of air via film cooling RDC aides in the consumption of the unburnt hydrogen. For the nitrogen case, the remaining hydrogen mass flow is less then the uncooled RDC partly because the increase in chamber pressure promotes more reaction in Region 1 and partly due to the increased mixing in Region 2. But the overall amount of remaining hydrogen is significantly more than the air film cooled case.

Correspondingly, a significant reduction in the outlet temperature was observed as the coolant mass flow increases. As reported in Table 3 for the uncooled combustor, the average exit temperature was 1900 K. With the film cooled RDC, for 40 g/s coolant flow (corresponding to P_{cool} = 2.75 bar) the temperature reduced to 1870 K. Similarly, for 3.0 bar with 68 g/s, the temperature reduced to 1840 K and is only 1771 K for P_{cool} = 3.5 bar with 112 g/s coolant mass flow. However, for 3.0 bar with nitrogen, the reduction is quite significant, the obtained temperature is 1760 K which is less then the 3.5 bar case with air. Clearly the coolant, which is entering the system at 300 K, was reducing the overall enthalpy of the exhaust. Without the additional secondary reactions that occur with air coolant, the nitrogen only acts to absorb heat.

However, the increase in temperature due to deflagration burning improved the combustion efficiency of the RDC (although it is not contributing to the pressure gain). The combustion efficiency was calculated using Eq. (2). The formula was derived using the enthalpy rise method i.e. the total enthalpy difference of the outlet to the inlet compared to the total heat addition [35]. As part of this development, the mass addition in the form of coolant was accounted for in the efficiency calculation as done in conventional gas turbine combustors.

$$\eta_c = \frac{C_{pg}\left(\dot{m}_a + \dot{m}_f + \dot{m}_c\right) T_{tout} \quad - \dot{m}_a C_{pa} T_{ta} - \dot{m}_f C_{pf} T_{tf} \quad - \dot{m}_{cool} C_{pcool} T_{tcool}}{LHV_f \dot{m}_f} \tag{2}$$

The combustion efficiency obtained using the expression is reported in Table 3. For the uncooled combustor, due to the 12.3% of unburnt hydrogen, the obtained efficiency was 90.5%. Whereas with film cooling, due to increased chamber pressure affecting the detonation and the coolant deflagration, the combustion efficiency increases. The increased efficiency corresponds with the reduction in the unburned hydrogen at the exit. The nitrogen coolant had a similar efficiency as the uncooled combustor, at 90.7% as there was only a slight reduction in the amount of unburned hydrogen. This further shows that inert gas has a small impact on additional reactivity due to enhanced mixing, but primarily just reduces the temperature in the combustor.

7. Conclusion

Rotating detonation combustors are high power density combustors with tremendous heat loads. Film cooling can be a possible solution for reducing these thermal loads. This study investigates the effects of film cooling on the performance of an RDC, specifically investigating the impact of secondary burning caused by the reaction of unburnt fuel with oxygen rich coolant. To study this at high fidelity, LES investigations were performed for a film cooled TU Berlin RDC using the AVBP solver. Three different plenum pressures were analysed namely 2.75, 3.0, and 3.5 bar which achieved three different coolant mass flows of 40, 68, and 112 g/s, respectively. Additionally, for the 3.0 bar case an investigation with nitrogen coolant was performed to distinguish between the effects of coolant mixing and the presence of oxygen on the levels of secondary burning.

The addition of film coolant increased the heat release in the detonation region and further modified the shape of the detonation. This was attributed to the increased chamber pressure caused by the addition of coolant mass flow. The coolant subsequently interacted with unburned hydrogen present in the oblique shock region and deflagrated. Higher jet penetration at higher coolant plenum pressures increased the mixing which enhanced the amount of secondary combustion. For the film cooled cases, nearly 60% of the unburnt hydrogen present at the film cooling starting location was consumed due to secondary burning. Whereas, the uncooled combustor only experienced around 30% of additional consumption downstream of the detonation wave.

An additional analysis was performed that compared the mixing between using nitrogen as the coolant versus air. As might be expected, both coolants were evenly mixed, however the air case consumed more of the available hydrogen. By comparing the nitrogen case to the uncooled case, the mixing due to the film had a small impact on the overall heat release. Nearly all the additional heat release could be attributed to the secondary burning that occurred due to the addition of air to the system. Overall, though, the additional air served to cool the combustor. A reduction of gas temperature up to 500 K was observed in the film cooled cases. Finally, the combustion efficiency was increased due to the secondary burning providing additional enthalpy to the core flow.

Overall, the results reveal that film cooling has a significant impact on the performance of an RDC. Locally, there was an increase in the gas temperature when using air as the coolant over an inert gas of nominally 100 K. However, these temperatures were 500 K lower than the uncooled condition. The addition of film cooling impacted the overall heat release through the combustor. Furthermore, the deflagration heat addition due to coolant burning helped in consuming the unburnt hydrogen and even increased the combustion efficiency of the RDC.

CRediT authorship contribution statement

Shreyas Ramanagar Sridhara: Writing – original draft, Supervision, Investigation, Conceptualization. **Antonio Andreini:** Supervision, Investigation, Funding acquisition. **Marc D. Polanka:** Writing – review & editing, Writing – original draft, Supervision, Investigation, Conceptualization. **Myles D. Bohon:** Supervision, Investigation.

Declaration of competing interest

The authors declare the following financial interests/personal relationships which may be considered as potential competing interests: Shreyas Ramanagar Sridhara reports statistical analysis and writing assistance were provided by University of Florence. Antonio Andreini reports a relationship with University of Florence that includes: employment, funding grants, and non-financial support. Marc D. Polanka reports a relationship with Air Force Institute of Technology that includes: non-financial support. Myles Bohon reports a relationship with TU Berlin University that includes: non-financial support. If there are other authors, they declare that they have no known competing financial interests or personal relationships that could have appeared to influence the work reported in this paper.

Acknowledgements

This project has received funding from the European Union's Horizon 2020 research and innovation program under the Marie Skłodowska-Curie grant agreement No 956803. The authors also thank Pier Carlo Nassini for his support.

Data availability

Data will be made available on request.

References

[1] Lee Jae Hyuk, Ryu Jae Hoon, Lee Eun Sung, Han Hyung Seok, Choi Jeong Yeol. Experimental proof of concept of a noncircular rotating detonation engine (RDE) for propulsion applications. Aerospace 2023;10(1). http://dx.doi.org/10.3390/aerospace10010027.

[2] Fiorino Nathan T, Snow Nathan J, Schauer Frederick R, Polanka Marc D, Schumaker S Alexander, Sell Brian C. Improving detonability in a small-scale rotating detonation engine using partial premixing. J Propuls Power 2023;39(2):232–41. http://dx.doi.org/10.2514/1.B38668.

[3] Bach Eric, Bohon Myles D, Paschereit Christian Oliver. Development of an instrumented guide vane set for RDC exhaust flow characterization. 2018, http://dx.doi.org/10.2514/6.2018-4479.

[4] Bach Eric, Paschereit C O, Stathopoulos Panagiotis, Bohon Myles D. An empirical model for stagnation pressure gain in rotating detonation combustors. Proc Combust Inst 2021;38(3):3807–14. http://dx.doi.org/10.1016/j.proci.2020.07.071.

[5] Andrus Ionio Q, Polanka Marc D, King Paul I, Schauer Fred R, Hoke John L. Experimentation of premixed rotating detonation engine using variable slot feed plenum. J Propuls Power 2017;33(6):1448–58. http://dx.doi.org/10.2514/1.B36261, URL https://arc.aiaa.org/doi/10.2514/1.B36261.

[6] Dechert Joseph R, Schauer Fred, Polanka Marc D, Schumaker S Alexander, Sell Brian C, Fotia Matthew L. Development of a small scale rotating detonation engine. In: AIAA scitech 2020 forum, vol. 1 PartF. January. 2020, p. 1–11. http://dx.doi.org/10.2514/6.2020-0127.

[7] Braun James, Sousa Jorge, Paniagua Guillermo. Numerical assessment of the convective heat transfer in rotating detonation combustors using a reduced-order model. Appl Sci (Switzerland) 2018;8(6). http://dx.doi.org/10.3390/app8060893.

[8] Goto Keisuke, Nishimura Junpei, Kawasaki Akira, Matsuoka Ken, Kasahara Jiro. Propulsive performance and heating environment of rotating detonation engine with various nozzles. J Propuls Power 2018;1–11. http://dx.doi.org/10.2514/1.B37196.

[9] Stevens Christopher A, Fotia Matthew L, Hoke John L. Quasi-steady heat transfer measurements in an RDE. AIAA SciTech Forum 2018;1–10. http://dx.doi.org/10.2514/6.2018-1884.

[10] Stevens Christopher A, Fotia Matthew L, Hoke John L. An experimental comparison of the inner and outer wall heat flux in an RDE. 2019, p. 1–15. http://dx.doi.org/10.2514/6.2019-1252.

[11] Sandri Umberto, Ramanagar S. Shreyas, Andreini Antonio, Myles Bohon D. Evaluation of cooling requirements for rotating detonation combustors. J Turbomach 2023;1–15. http://dx.doi.org/10.1115/1.4064260.

[12] Tian Jia, Wang Yuan-shuai, Zhang Jing-zhou, Tan Xiao-ming. Numerical investigation on flow and film cooling characteristics of coolant injection in rotating detonation combustor. Aerosp Sci Technol 2022;122:107379. http://dx.doi.org/10.1016/j.ast.2022.107379.

[13] Yu Jingtian, Yao Songbai, Li Jingzhe, Huang Yihui, Guo Chunhai, Zhang Wenwu. Effects of inlet and secondary flow conditions on the flow field of rotating detonation engines with film cooling. Int J Hydrog Energy 2022. http://dx.doi.org/10.1016/j.ijhydene.2022.11.354.

[14] Li Rui, Xu Jinglei, Lv Haiyin, Lv Dongdong, Song Jiazheng. Numerical investigations of the nozzle performance for a rocket-based rotating detonation engine with film cooling. Aerosp Sci Technol 2023;136:108221. http://dx.doi.org/10.1016/j.ast.2023.108221.

[15] Yu Jingtian, Yao Songbai, Li Jingzhe, Li Jianghong, Guo Chunhai, Zhang Wenwu. Numerical investigation of the rotating detonation engine with cat-ear-shaped film cooling holes under varying operating modes. Aerosp Sci Technol 2023;142(September):108642. http://dx.doi.org/10.1016/j.ast.2023.108642.

[16] Shen Dawen, Cheng Miao, Rong Guangyao, Sheng Zhaohua, Zhang Yunzhen, Wang Jianping. Effects of film cooling injection inclination angle on cooling performance in rotating detonation combustors. Phys Fluids 2024;36(2). http://dx.doi.org/10.1063/5.0188972.
[17] Scott Llewellyn Chriss. Characterization of a rotating detonation engine with an air film cooled outer body. [Ph.D. thesis], University of Dayton; 2022.
[18] Yu Jingtian, Yao Songbai, Li Jingzhe, Li Jianghong, Wang Rujia, Wang Bin, et al. Experimental verification of rotating detonation engine with film cooling. Phys Fluids 2024;36(3). http://dx.doi.org/10.1063/5.0200164.
[19] Meloni R, Nassini PC, Andreini A. Model development for the simulation of the hydrogen addition effect onto the nox emission of an industrial combustor. Fuel 2022;328(15):125278. http://dx.doi.org/10.1016/j.fuel.2022.125278.
[20] Nassini Pier Carlo, Andreini Antonio, Bohon Myles D. Characterization of refill region and mixing state immediately ahead of a hydrogen-air rotating detonation using LES. 2023;258. http://dx.doi.org/10.1016/j.combustflame.2023.113050.
[21] Schonfeld Thilo, Rudgyard Michael. Steady and unsteady flow simulations using the hybrid flow solver AVBP. AIAA J 1999;37(11):1378–85. http://dx.doi.org/10.2514/2.636.
[22] Gicquel Laurent YM, Gourdain N, Boussuge J-F, Deniau H, Staffelbach G, Wolf P, et al. High performance parallel computing of flows in complex geometries. C R Méc 2011;339(2–3):104–24. http://dx.doi.org/10.1016/j.crme.2010.11.006.
[23] Gicquel LYM, Staffelbach G, Poinsot T. Large eddy simulations of gaseous flames in gas turbine combustion chambers. Prog Energy Combust Sci 2012;38(6):782–817. http://dx.doi.org/10.1016/j.pecs.2012.04.004.
[24] Barré David, Kraushaar Matthias, Staffelbach Gabriel, Moureau Vincent, Gicquel Laurent YM. Compressible and low Mach number LES of a swirl experimental burner. C R Méc 2013;341(1–2):277–87. http://dx.doi.org/10.1016/j.crme.2012.11.010.
[25] Poinsot Thierry, Veynante Denis. Theoretical and numerical combustion. 2005.
[26] Dupuy D, Perrot A, Odier N, Gicquel LYM, Duchaine F. Boundary-condition models of film-cooling holes for large-eddy simulation of turbine vanes. Int J Heat Mass Transfer 2021;166:120763. http://dx.doi.org/10.1016/j.ijheatmasstransfer.2020.120763.
[27] Aillaud P, Duchaine F, Gicquel L Y M, Koupper C, Staffelbach G. Large eddy simulation of trailing edge cutback film cooling : Impact of internal stiffening ribs on the adiabatic effectiveness. In: 7th European Conference for Aeronautics and Aerospace Sciences, no. 1. 2017, p. 1–14.
[28] Shum-Kivan Francis, Duchaine Florent, Gicquel Laurent. Large-eddy simulation and conjugate heat transfer in a round impinging jet. In: Heat transfer. vol. 5A. American Society of Mechanical Engineers; 2014, p. 1–11. http://dx.doi.org/10.1115/GT2014-25152.
[29] Agarwal Shubham, Gicquel Laurent, Duchaine Florent, Odier Nicolas, Dombart Jérôme. Analysis of the unsteady flow field inside a fan-shaped cooling hole predicted by large eddy simulation. J Turbomach 2021;143(3):1–10. http://dx.doi.org/10.1115/1.4050121.
[30] Celik IB, Cehreli ZN, Yavuz I. Index of resolution quality for large eddy simulations. J Fluids Eng Trans ASME 2005;127(5):949–58. http://dx.doi.org/10.1115/1.1990201.
[31] Ramanagar Sridhara S, Andreini Antonio, Polanka Marc D, Bohon Myles D. LES investigation of film cooling in rotating detonation combustors . ASME - Turbomachinery Technical Conference and Exposition; 2024, http://dx.doi.org/10.1115/GT2024-123796.
[32] Polanka Marc D, Zelina Joseph, Anderson Wesly S, Sekar Balu, Evans Dave S, Lin Cheng Xian, et al. Heat release in turbine cooling I: Experimental and computational comparison of three geometries. J Propuls Power 2011;27(2):257–68. http://dx.doi.org/10.2514/1.45317.
[33] Anderson Wesly S, Polanka Marc D, Zelina Joseph, Evans Dave S, Stouffer Scott D, Justinger Garth R. Effects of a reacting cross-stream on turbine film cooling. J. Eng. Gas Turbines Power 2010;132(5):1–7. http://dx.doi.org/10.1115/1.3204616.
[34] Shewhart Andrew T, Polanka Marc D, Robertson Jacob J, Greiner Nathan J, Rutledge James L. Minimization of heat load due to secondary reactions in fuel rich environments. J. Eng. Gas Turbines Power 2015;137(12):1–10. http://dx.doi.org/10.1115/1.4030520.
[35] Lefebvre Arthur H, Ballal Dilip R. Gas turbine combustion alternative fuels and emissions. CRC press taylor & francis group, vol. 132, no. 11. CRC Press; 2010, p. 247–8. http://dx.doi.org/10.1201/9781420086058.